Journal of Materials Chemistry C

Accepted Manuscript

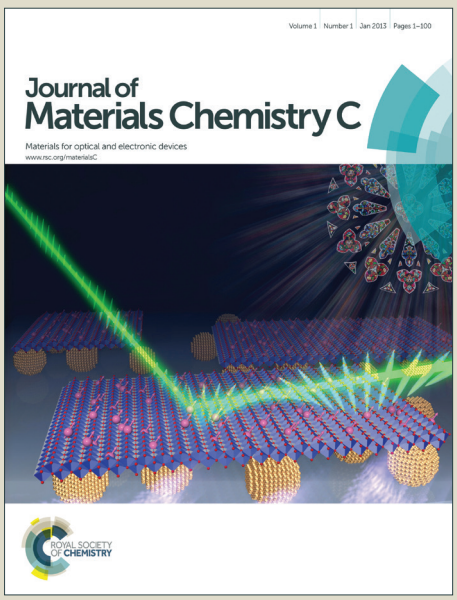

ROYAL SOCIETY OF CHEMISTRY

www.rsc.org/materialsC

Cite this: DOI: 10.1039/c0xx00000x

www.rsc.org/xxxxxx

ARTICLE TYPE

Fe-induced morphological transformation of 1-D CuO nanochains to porous nanofibers with enhanced optical, magnetic and ferroelectric properties

Umesh Kumar Gaur,[a] Anil Kumar[a,b] and G.D.Varma[b]

Received (in XXX, XXX) Xth XXXXXXXXX 20XX, Accepted Xth XXXXXXXXX 20XX
DOI: 10.1039/b000000x

The present work reports the synthesis of self- assembled 1-D polycrystalline Fe doped CuO nanostructures ($Cu_{1-x}Fe_xO$, x = 0.02 (SP2), 0.05 (SP5), 0.10 (SP10)) using wet chemical approach. The surface analysis of these nanostructures by x-ray photoelectron spectroscopy indicated Fe to be present as Fe^{3+}. The doping of Fe (2 to 10%) causes exchange of Cu in CuO and creates point defects - oxygen vacancies, which are manifested by: the change in morphologies of doped nanostructures from nanochains to nanofibers, a reduction in the size of CuO NPs from 19 to 5 nm, the red shifted optical absorption and fluorescence bands associated with an increase in the fluorescence lifetime(s) and blue shifted Raman spectra. The field dependent magnetization (M-H) measurements at room temperature show that for SP10 the magnetization value increases by a factor of about 3 as compared to that of undoped sample and superparamgnetic behavior increases with increasing Fe-content. Whereas, at 5 K it exhibits ferromagnetic behavior with increasing values of coercivity (1564 Oe) and retentivity (0.19 emu/g) and exchange bias effect decreasing with increased doping of Fe. The room temperature polarization versus electric field measurements at 200 Hz show weak ferroelectric behavior for all samples and increases with increasing Fe content in the sample. Dielectric constant and dielectric loss shows the decreasing value with increase in frequency. A correlation between the observed changes in morphology with optical, magnetic and ferroelectric properties upon doping of Fe has been analyzed.

Introduction

In recent years intense research has been carried on semiconducting oxide nanostructures (CuO, ZnO, TiO_2, NiO, SnO_2, Fe_2O_3 and Co_3O_4) because of their novel optical, magnetic and electric properties.[1,2] Among the oxides, a number of publications have focused on copper oxide nanostructures because of their narrow band gap and promising applications as bio sensors,[3,4] gas sensors,[5,6] photodetectors,[7] nanofluids,[8] field emissions,[9] energy efficient lubricent,[10] removal of inorganic pollutants,[11] photocatalysis[12] electrode material for Li-ion batteries[13] and supercapacitors.[14,15] Bulk CuO is known to exhibit antiferromagnetic[16] and multiferroic behavior at low temperature.[17] In recent years it has been observed that a control of the size, shape, dimensionality, and surface properties of nanostructures plays an important role in manipulating their ferroelectric[18] and magnetic behavior.[19]

CuO has earlier been synthesized in different dimensions (1-D, 2-D, 3-D), but 1-D nanostructures assume significant importance as regard to their increased efficiency for transport of electron and controlled optical and magnetic behavior which have applications in solar cell,[20,21] sensors, [22-24] FETs,[25] the next generation Na-ion batteries[26] and spintronics devices.[27] Recently, it was observed that the production of CuO nanochains induced the room temperature electric polarization along with a weak ferromagnetic interaction exhibiting short range magnetic ordering.[28] Lately, new materials are being developed to enhance room temperature polarization along with ferromagnetic properties for their potential in developing spintronic devices. Tun *et al*[29] observed room temperature multiferroic behavior in Cu doped ZnO. This behavior was also observed in V doped ZnO nanorods[30] and Cr doped ZnO thin films.[31] In pure ZnO nanorods[32] and thin films[33] defect induced ferroelectricity was observed. Recently, room temperature ferroelectric property was observed in high pressure CuO.[34] Hence, doping and defects are an efficient way to enhance magnetic and ferroelectric behavior of metal oxide nanostructures. Change in ferroelectric polarization can also be triggered by the specific magnetic order in Cu- oxide(s).[35]

In view of the above investigations, the present work focuses on examining the optical, magnetic and ferroelectric behavior of 1D CuO nanostructures in the presence of different amount of Fe dopant. Interestingly, the 10% doping of Fe into CuO produces fibrous nanostructures by creating point defects which enhance both polarization and dielectric constant significantly. The presence of point defects has been detected by fluorescence spectroscopy, lifetime measurements and Raman spectroscopy. The high aspect ratio and the porous structure of CuO nanofibers having high surface area lead to improved magnetic properties at

room temperature which may be interesting for their applications in memory devices.

Experimental

Chemicals

$Cu(NO_3)_2.3H_2O$, $Fe(NO_3)_2.6H_2O$, ethanol (Merck), ammonia solution (Thomas Baker), NaOH (SD Fine) were used for synthesis without any purification. Di-ionized (Milipore) water was used for all reactions.

Equipment

To measure the Zeta potential and hydrodynamic size a Zeta Sizer ZS90 (Malvern Instruments) equipped with 632 He-Ne laser was used. X-ray diffraction pattern of powdered samples were performed on a BRUKER D8 ADVANCE X-ray diffractometer using the Cu-Kα radiation (1.5418Å). Surface topography of the samples was recorded on NTEGRA atomic force microscope equipped with NOVA software using tapping mode. Morphology and elemental analysis were recorded on a field emission scanning electron microscope (FESEM) coupled with energy dispersive X-ray spectrometer (FEI- QUANTA 200FEG). HRTEM, selected area electron diffraction pattern and electron micrographs were recorded on a TECHNAI G2 20 S - TWIN transmission electron microscope (TEM). Absorption spectra were recorded on a SHIMADZU UV-VIS 2100S spectrophotometer. SHIMADZU RF-5301 PC was used for fluorescence measurements. Fluorescence lifetime measurements were recorded on a HORIBA JOBIN YVON fluoroCube fluorescence life time system equipped with nano LED source. The Raman spectra of powder sample were recorded on RENISHAW Raman spectrometer equipped with 514 nm Ar ion laser. Magnetic measurements were carried out on QUANTUM DESIGN MPMS-XL DC SQUID magnetometer. Ferroelectric measurement was performed on P-E loop Tracer. Frequency dependent dielectric measurements were made on a WAYNE KERR 6500 high frequency LCR meter**.** Digital pH meter from MICROSIL INDIA was used to measure the pH of solution. The Brunauer-Emmett-Teller (BET) surface area analysis of the Fe doped CuO samples were performed on NOVA 2200e High Speed Automated Surface Area Analyzer using Nova Win software by the adsorption and desorption of N_2 at 77K.

Methodology

Synthesis of Fe doped CuO nanostructures with compositions $Cu_{1-x}Fe_xO$ (x= 0.02, 0.05 and 0.10) were carried out by following our previously reported method.[28] In typical synthesis, the appropriate amount of cupric nitrate and ferric nitrate were mixed in 200 ml di-ionized water and stirred for 1 h for proper mixing of two salts. Thereafter 10 ml of ammonia solution was added into this solution rapidly under constant stirring. A blue precipitate of $Cu(OH)_2$ were obtained upon drop wise addition of NaOH and the pH was fixed between 11and 12. The blue precipitate was centrifuged and washed two times with distilled water and ethanol. Finally, the collected material was heated at 100˚ C for 10 h in air to synthesized Fe doped CuO nanostructures.

XRD, FESEM, Raman and SQUID measurements were performed using the powder samples. For FESEM study powder sample was applied on carbon tape which was put on an aluminum stub then gold was coated on the sample to make them conducting. For AFM measurements fresh sample was prepared on glass slides by drop casting method. Zeta sizer and optical measurements were designed by suspending a fix amount of powder in distilled water and sonicating it for about 10 min. For TEM measurements a small drop was applied on 300 mesh carbon coated copper grid and dried it at room temperature. Ferroelectric and dielectric measurements were made by coating silver on thin pallets of the sample. Thin Pallets of 8 mm dia were prepared using hydraulic press by applying a pressure of about 10 ton. The fluorescence decay curve was analyzed using the multi exponential iterative reconvolution technique, for which the software were provided by IBH. Data analysis was carried out by DAS 6.3 software. Henceforth, the samples doped with 2, 5 and 10 % Fe will be represented as SP2, SP5 and SP10, respectively.

Results

XRD analysis

XRD patterns of 2, 5 and 10 % Fe doped CuO samples are shown in Fig. 1(a). The patterns of all the samples correspond to monoclinic CuO up to doping level of 10 % and no extra diffraction peaks corresponding to Fe, FeO, Fe_2O_3 or Fe_3O_4 have been detected. However, for 15 % doping of Fe (Fig. S1), some peaks corresponding to α-Fe_2O_3 are also observed. This confirms that the solubility limit of Fe in CuO is up to 10 %. A careful examination of the intense peaks in these patterns reveals that with increasing Fe ion concentration the peaks get broadened and shifted towards higher angle (Fig. 1(b)) along with a decrease in their intensity.. Fig. 1(c) shows the variation of unit cell volume as a function of dopant concentration. This reveals that lattice parameter decreases with increasing doping concentration.

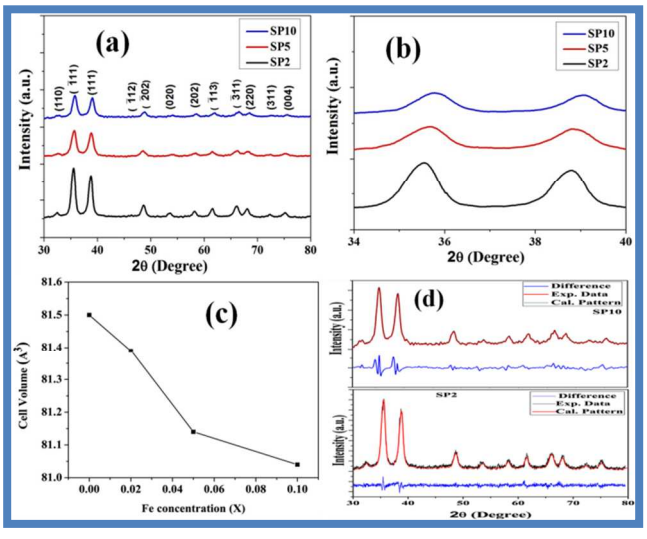

Fig. 1 (a) XRD pattern of SP2, SP5 and SP10. (b) Expanded view depicting two main peaks of SP2, SP5 and SP10. (c) Represent the change in unit cell volume with increased doping. (d) Rietveld refinement of 2 (SP2) and 10 % (SP10)) Fe doped samples.

Based on the XRD data, Rietveld refinement have been

presented for SP2, SP5 and SP10 by substituting some of the Cu ions by Fe ions in CuO lattice. Fig. 1(d) shows the typical refinement plots for SP2 and SP10. The fitted pattern is in agreement with the experimental data. Using this refinement, the lattice parameters for all the samples were calculated and the actual Fe ion concentration was estimated (Table-1). An examination of this table shows that the actual Fe ion concentration in SP2, SP5 and SP10 are slightly lower than those used for their preparation, which commonly occurs in synthesis process because of unavoidable loss. However, the decrease in lattice parameters with increasing Fe concentration indicates a little influence on the crystalline structure of CuO by the Fe substitution. All these finding indicate the uniform doping of Fe at Cu site(s) in CuO. Using Scherrer formula and full width at half maxima, the average particle size for SP2, SP5 and SP10 have been estimated to be ~ 15, 11 and 5 nm, respectively.

Table 1. Various parameters calculated from XRD refinement of SP2, SP5 and SP10

Sample	Fe concentration (%)	a (Å)	b (Å)	c (Å)	β (degree)
SP2	1.97	4.6835	3.4342	5.1291	81.39
SP5	4.94	4.6726	3.4312	5.1301	81.14
SP10	9.75	4.6672	3.4310	5.1301	81.04

The preferential orientation of nanoparticles along a crystal plane (hkl) in the sample was studied by calculating the texture coefficient of XRD peaks according to relation[36]

$$C_i = \frac{N\left(I_i/I_{i0}\right)}{\sum_{i=1}^{N}\left(I_i/I_{i0}\right)}$$

Where C_i is the texture coefficient of plane i, I_i is the measured integral intensity, I_{i0} the integral intensity from JCPDS file and N is the number of reflections in the x-ray diffraction pattern. The value of texture coefficient for $(\bar{1}11)$ plane was found to be greater than unity, while for all other peaks this was less than or equal to one.

XPS analysis

The surface of as synthesized CuO nanostructure containing 10 % Fe was analyzed by XPS. Panel (a) of Fig. 2 represents the XPS spectrum corresponding to Cu 2p core level. The Cu 2p core level splits into 3 peaks at 933.9, 942.5 and 954.2 eV corresponding to binding energy 2p1/2 and 2p3/2. This indicates Cu to be present in +2 valance state. The peak observed at 942.5 is assigned as the satellite peak for 2p3/2. The energy gap between 2p1/2 and 2p3/2 arises due to the spin orbit coupling. In panel (b) of Fig. 2 two main peaks located at 710.2 and 724 eV along with a satellite peak at 713.1 corresponding to Fe^{3+} are observed. The separation of 13.8 eV between two main peaks corresponds to spin-orbit coupling for Fe 2p1/2 and Fe 2p3/2. The satellite peak observed at 713.1 eV, which is shifted towards lower binding energy as compared to that of bulk sample, may be assigned to the Fe^{3+}. The panel (c) of Fig. 2 exhibits broad peak which could be resolved into two components. These peaks could be designated to O^{2-} present in CuO (529.4) and singly ionized oxygen vacancies (531.3 eV).[37]

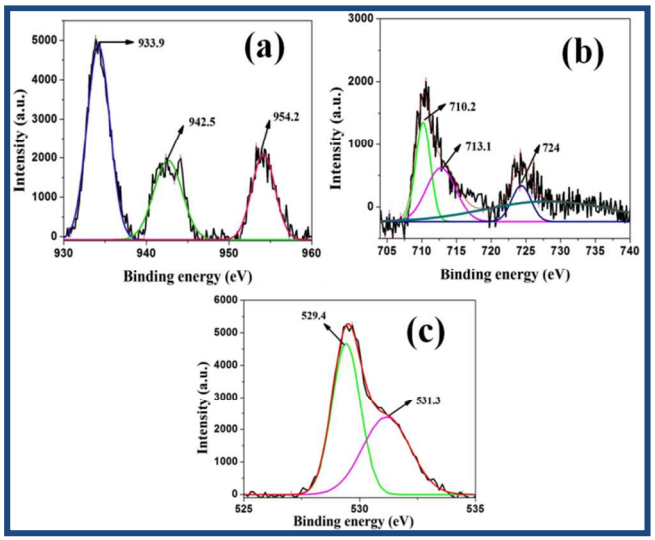

Fig. 2 XPS plots for SP10: (a) Cu, (b) Fe and (c) O.

DLS measurements

The stability of SP2, SP5 and SP10 were examined by measuring their zeta potential, which were found to decrease slightly with increased Fe doping (Fig. S2). However, these values remained constant even for the same sample dispersed in water after several days of its synthesis as well as by recording the zeta potential of the dispersed sample periodically for a period of about 3-4 days. The hydrodynamic size and size distribution of SP2, SP5 and SP10 was also measured using zeta sizer (Fig. 3). These plots exhibit mainly two fractions of nanostructures with a varied distribution of size. For SP2 the first fraction exhibits some small particles having range between (22-65 nm) and another fraction consists of size distribution of (100-900 nm) with an average size of 294 nm (Fig. 3(a)). An increase in Fe % (SP5) results in a decrease in the size for both the fraction with a slightly narrow size distribution. A further increase in the Fe % (SP10) makes this phenomenon more prominent as is apparent by the mixing of two fractions.

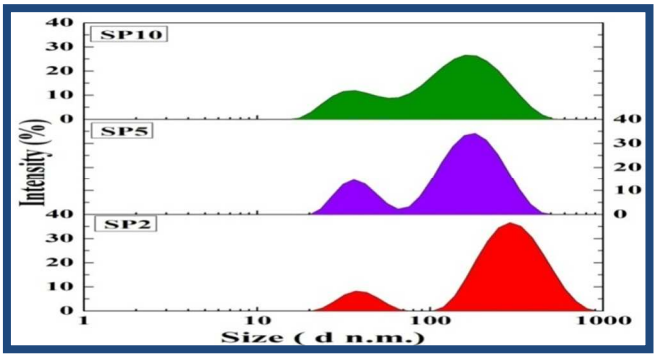

Fig. 3 DLS measurements showing variation of size distribution for SP2, SP5 and SP10.

FESEM analysis

The morphology of samples SP2, SP5 and SP10 was investigated

by recording their FESEM images. The FESEM image of sample SP2 shows the formation of network of CuO nanochains consisting of CuO nanoparticles (Fig. 4(a)). However, the FESEM images for SP5 and SP10 show the formation of fibrous nanostructures (see Fig. 4(b) and (c)) and the latter sample depicts the bundles of nanofibers with enhanced porosity (Fig. 4(c)). These results thus reveal that increased doping of Fe changes the morphology of CuO nanostructures from nanochains to nanofibers and nanofibers form bundles in the samples with higher Fe-content. Elemental mapping for a typical sample SP10 is presented in Fig. 4(d) and S3 which exhibits homogeneous distribution of Cu, Fe and O in these nanostructures.

AFM images (Fig. S4) also support the formation of chainlike topography for SP2 and fibrous bundles like topography for SP5 and SP10.

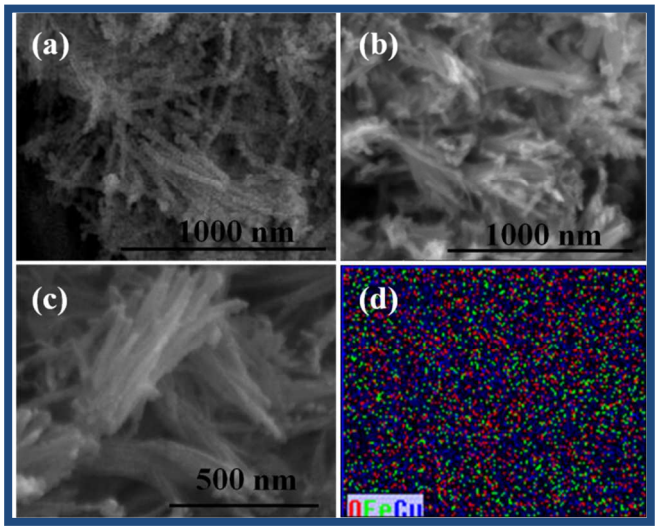

Fig. 4 FESEM images of: (a) SP2, (b) SP5, (c) SP10, (d) Elemental mapping for SP10.

TEM analysis

The size and morphology of CuO nanostructures was also determined by TEM. The TEM image of SP2 containing 2 % Fe shows the formation of nanochains consisting of nanoparticles with the average size of about 19 nm (Fig. 5(a)). An increase in Fe contents to 5 % results in the formation of clusters of fibrous nanostructures in which the average size of nanoparticles is reduced to about 10 nm (Fig. 5(b)). For the 10 % Fe doping the fibrous nature of nanostructures with increase porosity becomes quite apparent, in which the size of nanoparticles is further reduced to about 5 nm (Fig. 5(c)). SAED pattern of 10 % Fe doped sample is shown in Fig. 5(d). This pattern exhibits a number of concentric rings containing spots. The indexing of the rings pattern correspond to the planes (110), ($\bar{1}$11), (111), (202) and (113) matching with the JCPDS file number 5-0661. The HRTEM images of SP10 is shown in Fig. 5(e) which shows the presence of spherical nanoparticles containing the fringe with 'd' spacing of 0.25 nm corresponding to ($\bar{1}$11) plane. This plane was found to be the most intense plane in the XRD as well.

Surface area analysis

In view of the above changes in morphology from nanochains to nanofibers with doping of Fe, the BET surface area of SP2 and SP10 was determined by adsorption of N_2 gas following five point methods after degassing for 1 h at 80° C. The surface area of these samples was found to be 49 and 62 m^2/g, respectively. These values are 23 and 29 times higher as compared to that of bulk (2.16 m^2/g) CuO.[26]

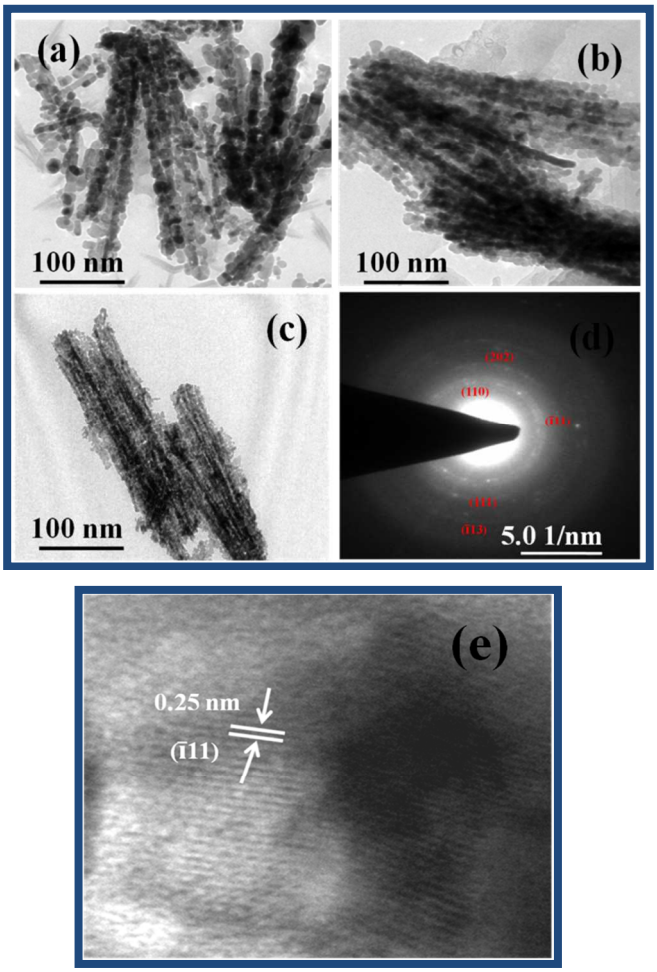

Fig. 5 TEM images: (a) SP2, (b) SP5, (c) SP10, (d) SAED pattern of SP10, (e) HRTEM image of SP10.

Growth mechanism

In the previous work it was observed that the undoped CuO, synthesized following the similar protocol, produces nanochains like structure. These nanochains were understood form by the adhesion of nanoparticles through non-covalent weak interactions. This has been manifested by the reduction in zeta potential with increased heating.[28] The change in morphology in present case upon doping of positively charged iron might be occurring due to the electrostatic interactions between the negatively charged CuO nanostructures and positively charged Fe^{3+} ions. These interactions result in the slight reduction in zeta potential upon 5 and 10 % Fe doping, which may be responsible for the formation of bundles of nanofibers. Further the doping of Fe causes exchange of Cu^{2+} by Fe $^{3+}$ which breaks the clusters of CuO nanoparticles into smaller units leading to the reduction in their size in nanochains/nanofibers. Remarkably, this growth

takes place in the absence of any surfactant.

Optical absorption and fluorescence studies

The effect of iron doping on the optical absorption behavior of CuO nanostructures was studied for all compositions of Fe as shown in Fig. 6. This figure shows a fairly prominent optical absorption band at 293 nm for the 2 % Fe doped sample, which is red shifted as compared to that of undoped CuO nanostructures[28] (278 nm). For 5 % and 10% doping of Fe the absorption bands get further red shifted to 305 nm and 334 nm, respectively. These results are different from the previous reports on nanoparticles[38] and nanowires/nanorods[39] in which the absorption peaks were observed at 280 and 375 nm, respectively. In pure CuO, the optical transition occurs directly from the valence band to the conduction band. However, the doping of Fe in 3 d state might create different surface states within the band gap of CuO. These surface states are possibly created due to oxygen vacancies and may be responsible for the observed red shifted behavior. Interestingly, for 15 % doping of iron this band gets significantly red shifted and is observed at 450 nm (Fig. S5).

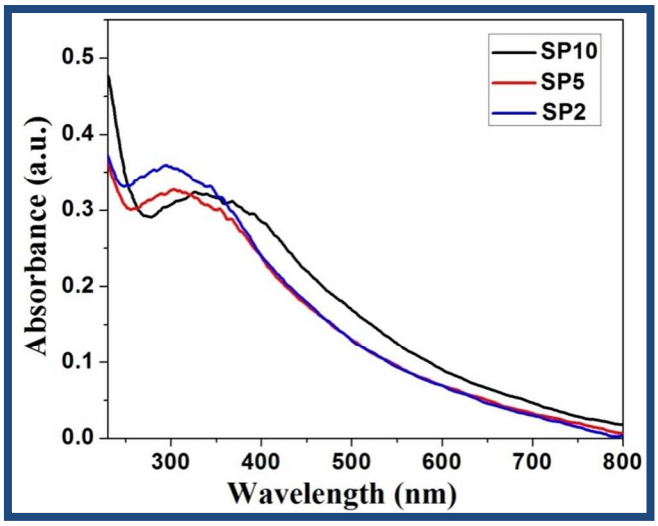

Fig. 6 UV-VIS absorption spectra of SP2, SP5 and SP10.

Since 5 % and 10 % doping of Fe results in a prominent change in the absorption behavior, more information about optical transition were analyzed by recording fluorescence spectra of these samples (Fig. 7). For both the samples the fluorescence spectra display three bands using excitation wavelength of 340 nm. For 5 % doped sample 3 peaks were recorded at 396, 432 (shoulder) and 509 nm (broad). An increase in doping of Fe to 10% further red shifted these bands to 400, 435 and 514 nm, respectively. However, the intensities of these bands are reduced with increased doping. These peaks have been assigned as the band edge emission, and bands arising due to two types of oxygen vacancies, i.e singly and doubly ionized oxygen vacancies, respectively.[40,41] In contrast to the undoped sample, the increased doping of Fe creates the varied population of different surface states within the band gap, which causes the increasing red shifted emission. The surface effect(s) and quantum confinement are among the most reported reasons, assigned to the blue and red shift in the optical phenomena.[42]

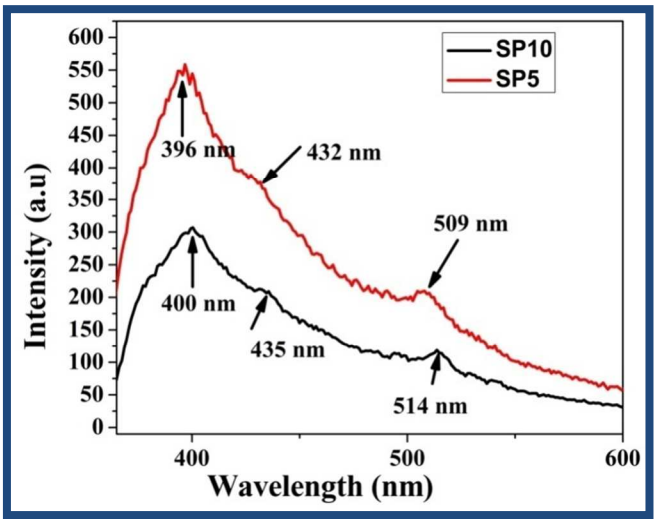

Fig. 7 Fluorescence spectra of SP5 and SP10.

In order to analyze the dynamics of charge carriers, the relaxation kinetics was monitored by recording the fluorescence lifetime for 10 % Fe doped sample by monitoring the fluorescence decay at all three wavelengths 400, 435 and 514 nm using 340 nm excitation light source (Fig. 8). The lifetime data for this sample are summarized in table 1. The lifetime is observed to increase with increasing emission wavelengths. A comparison of these data with those of undoped sample[28] shows that these lifetimes are higher for all the three emission energies and are longer at lower emission energies. Based on the different components of lifetime the depth of different surface states has been estimated using Arrhenius equation, in which the activation energy corresponding to the τ value of different components has been taken as the trap depth (Table 3).[43,44]

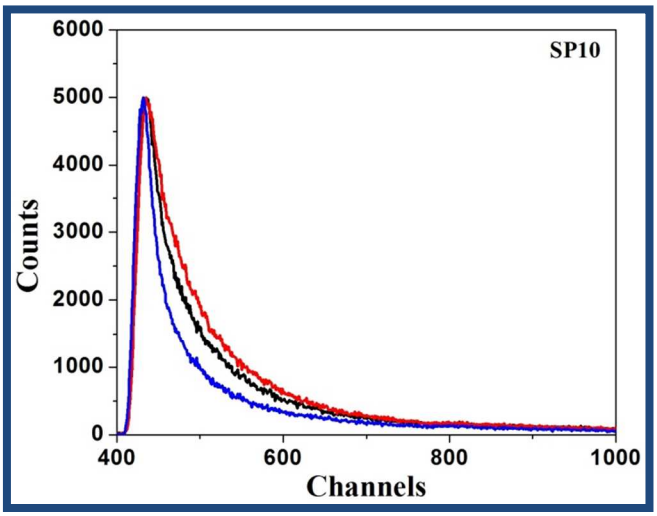

Fig. 8 Fluorescence decay curve for SP10 at different energies.

Raman spectra

The Raman spectra of different samples of Fe doped CuO (SP2, SP5, SP10) are shown in Fig. 9. An examination of these spectra reveals the three well known peaks (Ag, Bg and Bg)

corresponding to CuO in each case as observed earlier for undoped CuO nanochains thereby confirm its formation. An increase in the % Fe results the regular blue shift associated with a decrease in the intensity of all three Raman bands. Since there is a charge difference between Fe^{3+} and Cu^{2+}, the doping of Fe generates oxygen vacancies in the lattice of CuO to maintain the charge neutrality. Due to the generation of these oxygen vacancies, the lattice is contracted and peaks are shifted to higher wavenumber. It is also understood by the change in the morphology of CuO nanostructures for these samples which demonstrated growing fibrous nature of these nanostructures with increasing Fe doping.

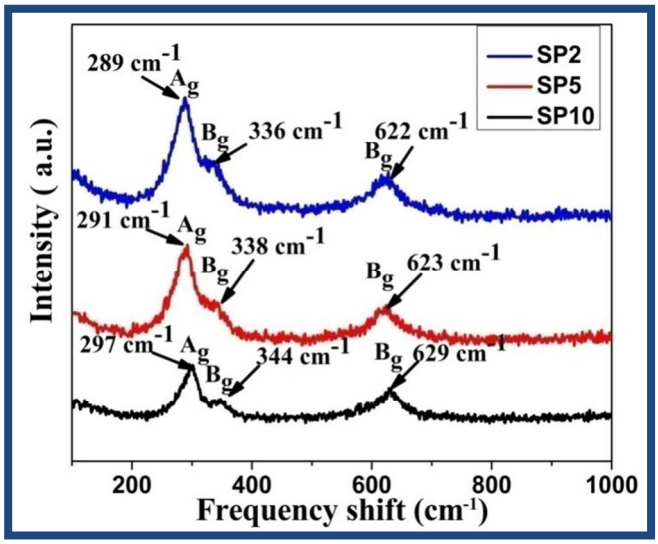

Fig. 9 Raman spectrums of SP2, SP5 and SP10.

Magnetic analysis

M-H plots for SP5 and SP10, recorded at 300 K, are shown in Fig. 10 (a). A comparison of the value of magnetization for these curves with that of undoped CuO nanostructures, recorded under similar conditions, shows that the magnetization increases with increasing doping of Fe. For 10 % Fe doping the value of magnetization is increased by a factor of about 3. Moreover, these M-H curves show the absence of hysteresis loop without any coercivity (H_c) and remanance (M_r). The non-saturation in magnetization in these curves indicates superparamegnetic behavior with paramagnetic component for both the samples. In order to analyze the superparamagnetic (SPM) and paramagnetic (PM) contribution(s) to the magnetic moment, the experimental data were fitted to Langevin function with an added linear paramagnetic term.[45]

$$M(H) = M_S^{SPM}\left[\coth\left(\frac{\mu H}{kT}\right) - \left(\frac{\mu H}{kT}\right)^{-1}\right] + C^{PM}H$$

Where, M_S^{SPM} is the saturation magnetization of SPM part, μ is the average magnetic moment and C^{PM} is the susceptibility of paramagnetic component.

The experimental plots and fitted curves for SP5 and SP10 up to ± 1 T are displayed in Fig. 10 (c) and 10 (d), respectively. It can be seen that for SP5, SPM contribution is only 6 % of the total magnetization, while rest 94 % comes from paramagnetic component. On the other hand for sample SP10, SPM contribution is increased to 14 % and the remaining 86 % is contributed from the paramagnetic components. Thus superparamagnetic component increases with increasing Fe-doping concentration in the sample.

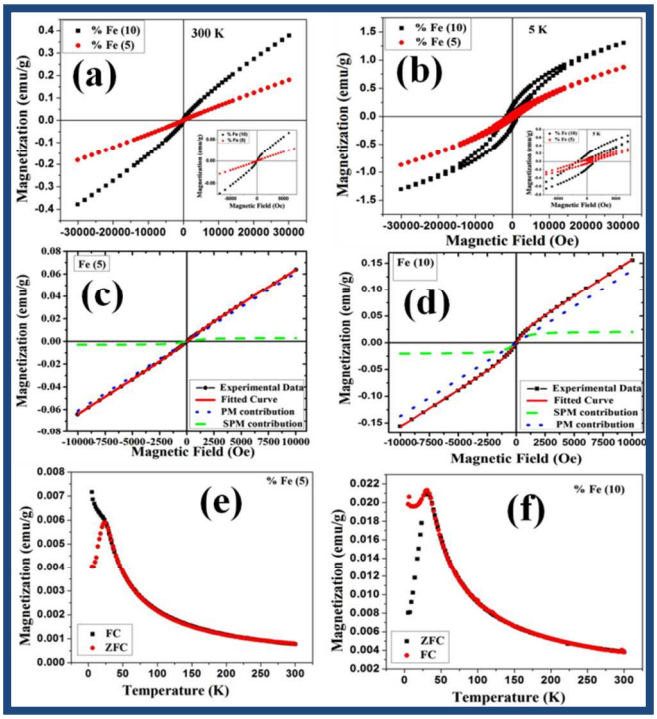

Fig. 10 (a) M-H plots for SP5 and SP10 at room temperature. Inset shows the expand view, (b) M-H plots for SP5 and SP10 at 5 K. Inset shows the expand view.(c, d) Fitted M-H curves at room temperature for SP5 and SP10 up to ± 1 T (e) FC-ZFC plot for SP5. (f) FC-ZFC plot for SP10.

The M-H curves of samples, SP5 and SP10, measured at 5 K under FC condition are shown in Fig. 10(b). We see that at low temperature, magnetic behavior changes from superparamagnetic to ferromagnetic with the development of H_c (1074 Oe) and M_r (0.05 emu/g) for SP5 and H_c (1564 Oe) and M_r (0.19 emu/g) for SP10. A careful analysis of these curves further reveals a slight shifting in hysteresis loop possibly due to the exchange bias effect. The observed values of exchange biases are 32 and 20 Oe for SP5 and SP10, respectively. However, these estimated values of exchange biases for Fe-doped CuO nanostructures are significantly lower than that of undoped CuO nanostructure (290 Oe).

The FC-ZFC (M-T) curves for samples SP5 and SP10, recorded at 100 Oe, are shown in Fig. 10(e, f). Both of these curves display distinct irreversibility between FC and ZFC curves at 24 K and 32 K, respectively. These points correspond to the blocking temperature (T_B) of these samples and are associated with the particle size and surface anisotropy. A comparison of T_B of doped samples with that of undoped one (56 K) again indicates that the blocking temperature decreases with Fe-doping, and follow the order $T_B(CuO) > T_B(SP5) < T_B(SP10)$. The value of magnetization is also significantly higher in M-H plots, measured at 5 K (i.e. below T_B) as compared to those of at room temperature. FC curves for SP5 and SP10 follow the same trend up to about 50 K and, thereafter, these curves show different behavior. This may be due to the increased surface effects and the

fibrous nature of SP10. Such behavior has also been observed earlier in the hollow nanostructures.[46] Fig. (S6) shows the FC magnetization versus temperature plots fitted with Curie-Weiss law. These fitted curves follow Curie- Weiss law only at high temperature (< ~25 K).

Ferroelectric and dielectric data

The ferroelectric behavior of SP5 and SP10 were examined by measuring the ferroelectric loops using P-E loop tracer at room temperature and 200 Hz (Fig. 11). Both the samples exhibit the formation of weak ferroelectric loops at room temperature. From these loops the remnant polarization (P_r) and electric coercivity (E_c) at 200 Hz for SP5 and SP10 were determined to be 1.74 μC cm^{-2} and 1.47 kV cm^{-1} and 2.97 μC cm^{-2} and 1.61 kV cm^{-1}, respectively. It shows that the values of P_r and E_c to increase with increasing doping. In a previous report CuO having spiral spin structure with large superexchange interactions has been considered to produce induced multiferroics with high T_c.[17] The doping of certain other dopants, like Zn and Ni causing exchange with Cu^{2+}, have been observed to result in the magnetic ordering in CuO.[47,48] Similar effects might be responsible for increase magnetic ordering in the present case due to creation of oxygen vacancies by the doping of Fe and, hence, result in the enhancement in ferroelectricity.

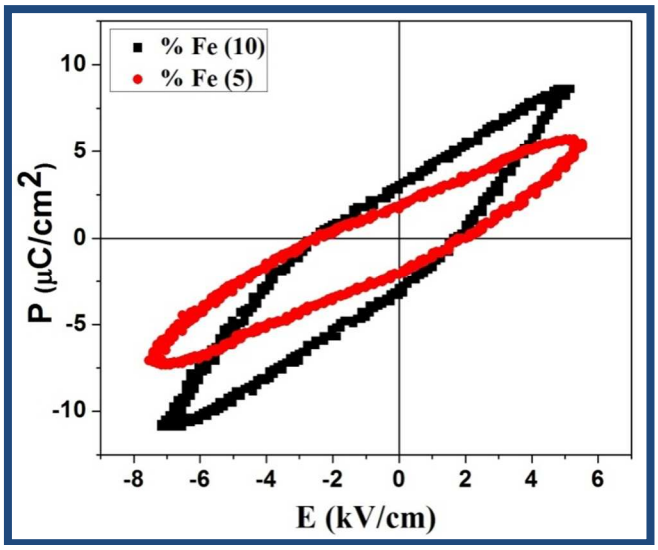

Fig. 11 P-E loops of SP5 and SP10.

The increased polarization for SP10 suggests that it contains more number of defects as compare to SP5. A careful examination of these loops shows the observed P-E loops to be asymmetric and the asymmetric behavior for SP10 to be higher as compared to that of SP5.

For samples SP5 and SP10 the dielectric constant (ε) was also determined using the relationship $\varepsilon = Cd/\varepsilon_o A$, where C is the capacitance, d is the thickness, ε_o is permittivity of free space and A is the surface area of the sample. The ε versus frequency curves are shown in Fig. 12 (a, c). These curves exhibit the higher value of dielectric constant at low frequency. A comparison of the dielectric constant value of doped samples with that of undoped one shows that dielectric constant increases with increasing doping of Fe, i.e follow the order: ε (SP10) > ε (SP5) > ε (SP1) (CuO nanochains). The observed larger value of dielectric constant is understood by the decreased particle size with Fe doping, which would enhance grain boundaries resulting in an increase in the dipole moment per unit volume.[30] The dielectric loss versus frequency curves are shown in Fig. 12 (b, d). A careful analysis of these curves show the decay is faster for SP5 in comparison to that of SP10 suggesting dielectric loss to reduce with increased doping of Fe.

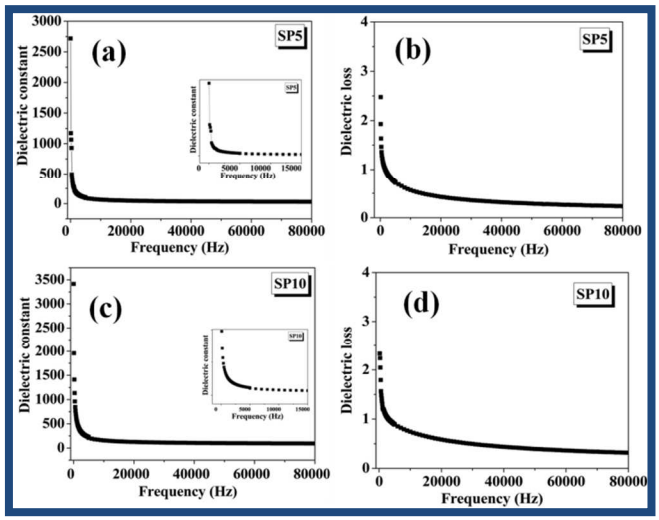

Fig. 12 (a) Dielectric constant *vs* frequency plot for SP5, Inset shows the expanded view (b) Dielectric loss *vs* frequency plot for SP5. (c) Dielectric constant *vs* frequency plot for SP10, Inset shows the expanded view (d) Dielectric loss *vs* frequency plot for SP10.

Discussion

An increase in the doping of Fe from 2 to 10 % in CuO results in a change in its morphology from nanochains to nanofibers as was evidenced by AFM (Fig.S4), FESEM (Fig. 4) and TEM (Fig. 5) analyses. This change in morphology is supported by BET analysis in which the surface area (m^2/g) for SP10 (62) was about 25% higher to that of SP2 (49) and about 4.7 times higher to those of nanowires.[26] In these samples CuO exhibits the formation of polycrystalline monoclinic structure as was evidenced by SAED (Fig. 5(d)) and XRD analyses (Fig. 1). The spacing in HRTEM fringes correspond to $(\bar{1}11)$ plane and the same plane found to be the most intense in the XRD with a texture coefficient > 1, thus indicating the growth of these nanostructures along this plane. In contrast to the undoped CuO nanochains, the doping of Fe^{3+} may either bring substitution of Cu^{2+} of CuO or gets incorporated as interstitial but because of the smaller ionic radius of Fe^{3+} (0.064 nm) as compared to that of Cu^{2+} (0.073 nm), Fe^{3+} is likely to exchange Cu^{2+} resulting in the introduction of point defects-oxygen vacancies in CuO. Furthermore, an increase in doping of Fe^{3+} results in a decrease in the size of CuO nanoparticles along with a decrease in intensity of XRD peaks which suggests the introduction of more defects[49] in CuO with increasing Fe ions contents. It is also reflected in the decrease in the lattice parameters and unit cell volume because of more substitution of Fe for Cu with increasing Fe ions contents. A reduction in the size and narrow size distribution of CuO NPs is also evidenced by TEM analysis and hydrodynamic radius measurements of the doped dispersion (Fig. 3). A very similar observation has earlier been made in case of Fe^{3+} doped NiO

nanostructures.[50] However, the particle size(s) measured from DLS are much bigger as compared to those observed from XRD and TEM techniques. This might have arisen due to the fact that DLS measurement gives the hydrodynamic size, whereas, from XRD data using Debye-Scherrer equation one determines the crystallite size. The difference in TEM and DLS measurements might have been contributed due to non-spherical morphology of nanostructures[51] and different methodologies adopted for sample preparation in these measurements. Elemental mapping of SP10 demonstrated a homogeneous distribution of Cu, Fe and O in these nanostructures (Figs. 4 d and S3). The uniform dissemination of Fe all along the nanofibers causing a reduction in the size of CuO NPs evidently suggests its participation in the observed morphological transformation.

Table 2. Lifetime measurement for SP10 at different emission energies.

Emission wavelength (nm) (Energy (eV))	Lifetime (ns)							
	Component1		Component 2		Component 3		<τ> (ns)	χ2
	τ1	Emission %	τ2	Emission %	τ3	Emission %		
400 (3.09)	2.75 (49.39)	35. 96	14.1 (253.25)	35.25	0.14 (2.65)	28.79	7.8	1.19
435 (2.84)	3.7 (67.10)	58.23	0.23 (4.13)	14.71	13.92 (249.89)	27.06	8.9	1.12
514 (2.40)	3.49 (62.71)	51.21	15.37 (275.92)	30.52	0.21 (3.93)	18.27	13.6	1.17

The formation of nanochains in the absence of any doping has been considered to occur through the adhesion of nanoparticles involving weak van der Waals forces among them.[28] Obviously, the doping of Fe results in the breaking of these CuO nanoclusters into smaller units upon the exchange of Cu^{2+} by Fe^{3+}. The observed change in morphology from chains to fibrous is thus understood due to the changed interactions among smaller sized Fe^{3+} doped CuO units. The reduced interaction among CuO nanoclusters in nanochains is also indicated by the reduction in zeta potential value with increased doping of Fe^{3+} (Fig. S2).

In contrast to the undoped sample, the doping of Fe brings a regular red shift in its optical absorption band with increased doping concentration suggests the creation of surface states within the band gap (Fig. 6). Interestingly, for 15% doping of iron the optical absorption band is further shifted to the red region having absorption maximum at 450 nm, which corresponds to the absorption due to α- Fe_2O_3.[52] It, thus suggests the possibility of the formation of α-Fe_2O_3 as Fe doping concentration exceeds 10%. The formation of α-Fe_2O_3 in 15 % Fe doped sample could be confirmed by the XRD (Fig. S1). This implies that the solubility limit of Fe in the present CuO nanosystem is below 15 %, which is similar to the estimation made earlier for CuO nanosytems.[53,54] Similarly, an increased doping of Fe brings a regular red shift in the emission bands observed at 390, 410 and 440 nm in the absence of Fe (Fig. 7). However, the intensity of emission bands is reduced with increased doping. From these changes it can be inferred that the doping of Fe creates non-radiative centre(s) in CuO along with the deeper traps located at lower energy. The presence of defects is also supported by time-resolved fluorescence spectroscopy in which the fluorescence decay at lower energies exhibits longer lifetimes (Fig. 8), as compared to that of the undoped sample.[28] It clearly manifests the creation of defects at lower energy. The presence of defects is further evidenced by XPS data in which a shoulder in O 1s peak is observed at 531.3 eV (Fig. 2, panel c). This peak has earlier been assigned to singly ionized oxygen vacancies for CuO.[37] The observed blue shift in all Raman band upon doping of iron is understood to occur due to the exchange of Cu^{2+} ions by higher valent Fe^{3+} (Fig. 9) and can be assigned to the confinement of phonon in the lattice and presence of oxygen vacancies. Similar changes in Raman bands have earlier been observed for NiO system.[50] The exchange of Cu by Fe is also supported by XRD measurements in which a decrease in unit cell volume and a slight shift in reflections due to different planes towards higher angle were observed.

Table 3. Energy of trap state for SP10 corresponding to different τ values (meV)

Emission wavelength (nm)	Energy of trap state corresponding to different τ values (meV)		
	τ_1	τ_2	τ_3
400	264	305	187
435	272	200	306
514	269	309	197

It is interesting that the magnetization is enhanced with doping of Fe and for SP10 it is about 3 times higher to that of pure CuO. It is understood by the combined effect of increased: (i) defects due to Cu^{2+} substituted by Fe^{3+} in these nanostructures. (ii) total spins of 'd' electrons.[55] An analysis of the magnetization data reveals it to contain the contribution from both the paramagnetic and superparamagnetic components. The observed change in magnetic behavior may be attributed to the transformation of the morphology from nanoparticles to nanofibers *via* nanochains. This evidently suggests relatively higher fraction of surface spins in nanofibers. Another consequence of increased doping of Fe is a decrease in exchange bias and increase in H_c compared to that of undoped CuO. This behavior can be appreciated by the fact that the bulk CuO is antiferromagnetic at low temperature and the doping of Fe introduces the ferromagnetic behavior in these

nanostructures causing a regular decrease in the exchange bias with increasing Fe. Although the doping of Fe enhances ferromagnetic interaction in the samples, however, the non saturated M-H loops observed in the present case still indicate the presence of antiferromagnetic phase. Thus it is concluded that both antiferromagnetic and ferromagnetic phases are responsible for observed magnetic behavior at low temperature.

The values of T_B follow the complex order: SP5 < SP10 > CuO nanochains. The lowering of T_B (24 K) for SP5 as compared to that of undoped CuO nanochains (56 K) has been assigned to the decrease in particle size for the present nanosystem. However, the higher value of T_B (32 K) for SP10, despite of its particle size being lower to that of SP5, can be assigned to the increase porosity in SP10 as compared to that of SP5. It essentially enhances the surface effects and contributes to the surface anisotropy in SP10. Similar behavior was observed earlier for hollow iron oxide nanoparticles.[56]

A distinct separation between FC and ZFC curves at low temperature, as is revealed by an increase in the magnetization value for the ferromagnetic component in SP10 (Fig. 10), suggests it to have arisen due to the uncompensated surface spins at low temperature due to larger surface effects and enhanced surface anisotropy . Such a phenomenon may also be contributed due to the change in morphology for SP10 from nanochains to nanofibers. A very similar behavior has earlier been reported for Fe doped NiO nanostructures.[57]

The higher values of polarization and dielectric constant in SP5 and SP10 as compared to that of bulk CuO[17] as well as pure CuO nanochains is understood by an increase in dipolar character upon doping of Fe. Doping of Fe^{3+} at Cu^{2+} site makes excess of defect state in system and this plays an important role in enhancing the polarization.[58]The observed decrease of dielectric constant with increased frequencies (Fig. 12) can be explained due to the non availability of enough time for reorganization of charge carriers with respect to an external field, and makes the dielectric constant to be independent of frequency at their higher values. On the other hand relatively low dielectric loss in SP10 can be ascribed to the increased number of defects in this sample. The presence of the increased number of defects is also evidenced by optical and fluorescence spectroscopic data, where increased doping resulted in a regular red shifting of optical absorption (Fig .6) and fluorescence bands (Fig. 7), respectively. This observation is also supported by the regular blue shifted Raman bands associated with a decrease in their intensity. Even a comparison of dielectric loss for SP10 with SP5 exhibits the low dielectric loss in the former, suggesting the role of doping in controlling the process of dielectric loss. This finding can be explained by a change in the charge carrier dynamics upon doping as is also evidenced by fluorescence lifetime measurements. In fact the doping causes the generation of more oxygen vacancies for SP10 which trapped the recombine space charges and hence increase the polarization and dielectric constant. The observed change(s) in various properties upon doping of Fe can also be contributed partially to the change in size, shape, and morphology of these nanostructures as has been observed earlier.[2,38-40,42,]

Conclusions

In summary, low dimensional Fe^{3+} doped CuO nanostructures with monoclinic structure have been synthesized successfully following wet chemical method. XRD and HRTEM images indicate that the growth of these nanofibers takes place along $(\bar{1}11)$ plane unlike to those of bulk, which exhibits the most intense diffraction band corresponding to (111) plane. Shifting of XRD peaks towards higher angle associated with decrease in unit cell volume reveals the uniform doping of Fe at Cu site(s) in CuO. Optical, fluorescence and Raman spectroscopy reveal increasing creation of point defects-oxygen vacancies with increased doping of Fe. Longer fluorescence lifetime also supports this finding. Room temperature superparamagnetic behavior with higher magnetization value has been assigned to the increased number of defects and total spins due to 'd' electrons. The lowering of blocking temperature (T_B) as compared to that of undoped CuO nanochains (56 K) has been assigned to the decrease in particle size and also the morphologies for the present nanosystems(s), which was also revealed by TEM analysis. At low temperature the hysteresis loop with slight exchange bias indicated the higher surface/shape anisotropy. The Fe doped fibrous CuO nanostructures with enhanced ferroelectric and dielectric behavior might be of great importance in microelectronics as capacitor and memory devices. To best of our knowledge the observed value of polarization and dielectric constant are the highest for CuO based 1-D nanostructures.

Acknowledgements

Umesh Kumar Gaur is grateful to CSIR (Government of India), New Delhi, for the award of fellowship.

Notes and references

[a] *Centre of Nanotechnology, Indian Institute of Technology Roorkee,* Roorkee-247667, India
[b] *Department of Chemistry, Indian Institute of Technology Roorkee,* Roorkee-247667, India
[c] *Department of Physics, Indian Institute of Technology Roorkee, Roorkee-247667, India*

1 R. S. Devan, R. A .Patil, J. H. Lin and Y. R. Ma, *Adv. Funct. Mater.*, 2012, **22**, 3326
2 S. Zoolfakar, R. A. Rani, A. J. Morfa, A. P. O'Mullane and K.K. Zadeh, *J. Mater. Chem. C*, 2014, **2**, 5247
3 S. Sun, Xi. Zhang, Yu. Sun, S. Yang, Xi. Song and Z. Yang, *ACS Appl. Mater. Interfaces*, 2013, **5**, 4429
4 O. Akhavan and E. Ghaderi, *J. Mater. Chem.,* 2011, **21**, 12935
5 R. H. Bari, S. B. Patil and A. R. Bari, *International Nano Letters*, 2013, **3,** 12
6 J. Deng, Li. Wang, Z. Lou and T. Zhang. *J. Mater. Chem. A,* 2014, **2,** 9030
7 W. Tian, C. Zhi, T. Zhai, Xi Wang, M. Liao, S. Li, S. Chen, D. Golberg and Y. Bando, *Nanoscale,* 2012, **4,** 6318
8 M. S. Kwasny, L. Chancelier, S. Ng, H. G. Manyar, C. Hardacre and P. Nockemann, *Dalton Trans.*, 2012, **41,** 219
9 Z. Liao, W. D. Zhu, J. B. Chen, X. Q. Zhang, and C.W. Wang, *Journal of Alloys and Compounds*, 2014, **609**, 253
10 R. Gusain and O. P. Khatri, *J.Mater. Chem.A*, 2013, **1,** 5612
11 P. K. Raul, S. Senapati, A. K. Sahoo, I. M. Umlong, R. R. Devi, A. J.Thakur and V. Veer, *RSC Adv.*, 2014, **4,** 40580
12 G. A. Naikoo, R. A. Dar and Farid Khan, *J. Mater. Chem. A,* 2014, **2,** 11792

13 C. Wang, Q. Li, F. Wang, G. Xia, R. Liu, D. Li, N. Li, J. S. Spendelow, and Gang Wu, *ACS Appl. Mater. Interfaces* 2014, **6,** 1243

14 M. J Deng, C. C. Wang, P J. Ho, C. M. Lin, J. M. Chen and K.T. Lu, *J. Mater. Chem. A,* 2014, **2,** 12857

15 G. S. Gund, D. P. Dubal, D.S. Dhawale, S.S. Shinde and C. D. Lokhande, *RSC Adv*., 2013, **3,** 24099

16 Y. Zhang, L. Pan, Y. Gu, F. Zhao, H. Qiu, J. Yin, H. Zhu and J.Q. Xiao, *J. Appl. Phys.,* 2009, **105,** 086103

17 T. Kimura, Y. Sekio, H. Nakamura, T. Siegrist and A. Ramirez, *Nature Materials,* 2008, **7,** 291

18 J. Varghese, R.W. Whatmore and J.D. Holmes, *J. Mater. Chem. C,* 2013, **1**, 2618

19 V. P. Thakare, O. N. Game and S.B. Ogale, , *J. Mater. Chem. C,* 2013, **1**, 1545

20 A. Bhaumik, M. Shearin, R. Patel and K. Ghosh, *Phys.Chem.Chem.Phys.,* 2014, **16,** 11054

21 T. Garcia-Esparza, K. Limkrailassiri, F. Leroy, S. Rasul, W. Yu, Li. Lin and K. Takanabe*, J. Mater. Chem. A*, 2014, **2**, 7389

22 X. Gou, G. Wang, J. Yang, J. Park and D. Wexler, *J.Mater. Chem.,* 2008, **18,** 965

23 X. Li, Y. Wang, Yu Lei and Z. Gu, *RSC Adv.,* 2012, **2,** 2302

24 S. W. Choi, A. Katoch, J. H. Kim and S. S. Kim, *J. Mater. Chem. C.* 2014, **2,** 8911

25 M. Vaseem, A. R. Hong, R. T. Kim and Y.B. Hahn, *J. Mater. Chem. C*, 2013, **1,** 2112

26 L. Wang, K. Zhang, Z. Hu, W. Duan, F. Cheng, and J. Chen, *Nano Research* 2014, **7(2),** 199

27 D.M. Gillingham, C.Muller, J Hong, R Q Wu and J A C Bland, J. Phys.: Condens. Matter, 2006, **18,** 9135

28 U. K. Gaur, A. Kumar, and G. D. Varma, CrystEngComm, 2014, **16**, 3005

29 T. S. Herng, M. F. Wong, D. Qi, J. Yi, A. Kumar, A. Huang, F. C. Kartawidjaja, S. Smadici, P. Abbamonte, C. S. Hanke, S. Shannigrahi, J. M. Xue, J. Wang, Y.P. Feng, A. Rusydi, K. Zeng, and J. Ding, Adv. Mater. 2011, **23,** 1635

30 M. K. Gupta and B. Kumar, J.Mater.Chem., 2011, **21**, 14559

31 Y. C. Yang, C. F. Zhong, X. H. Wang, B. He, S. Q. Wei, F. Zeng and F. Pan, J.Appl. Phys.,2008, **104,** 064102

32 M. Ghosh and G. M. Rao, Sci. Adv. Mater.2013, **5,** 1

33 Y. H. Lin, M. Ying, M. Li, X. Wang and C.W. Nan, Appl. Phys. Lett.,2007, **90,** 222110

34 X. Rocquefelte, K. Schwarz, P. Blaha, S. Kumar and J. van den Brink, *Nature Comm.,* 2013, **4,** 2511

35 X. Rocquefelte,, K. Schwarz and P. Blaha, *Scientific Reports*, 2012, **2,** 759

36 X. Mathew and J. P. Enriquez, *J. Appl. Phys*. 2006, **100**, 073907

37 D.Gao, G.Yang, J.Li, J.Zhang, J.L.Zhang and D.Xue, *J. Phys. Chem C*, 2010, **114**, 18347

38 W. Chen, J.Chen, Y.B.Feng,L.Hong, Q.Y.Chen, L.F.Wu, X.H. Lin and X.H.Xia, *Analyst*, 2012, **137**, 1706

39 L.Wang, Q.Zhou, G.Zhang, Y.Liang, B.Wang, W.Zhang, B.Lei and W.Wang, *Materials Letters*, 2012, **74**, 217

40 N.Mukherjee, B.Show, S.K.Maji, U.Madhu, S.K.Bhar, B.C.Mitra, G.G.Khan and A.Mondal, *Materials Letters,*2011, **65,** 3248

41 Y.Wang, T.Jiang, D.Meng, J.Kong, H.Jia and M.Yu, *RSC Adv.* 2015, **5,** 16277

42 Q.Zhang, K.Zhang, D.Xu, G.Yang, H.Huang, F.Nie, C.Liu and S.Yang, *Prog. Mater.Sci.,* 2014, **60**, 208

43 A.Eychmuller, A.Hasselbarth, L.Katsikas and H.Weller, *J.Luminiscence,* 1991, **48-49,** 745

44 A.Kumar and B.Singh, *Dalton Trans.* 2013, **42,** 11455

45 H. Khurshid, W. Li, M. H Phan,P. Mukherjee, G.C.Hadjipanayis and H. Srikanth, *Appl. Phys. Lett.,* 2012, **101,** 022403

46 H. Khurshid, W. Li, M. H Phan,P. Mukherjee and H. Srikanth, *Appl. Phys. Lett*., 2014, **104**, 072407

47 T.I.Arvuzova, I.B.Smolyak, S.V.Noumov and A.A.Samokhvalov, *Phys. Solid State*, 1998, **40**, 1702

48 J.Hellsvik, M.Balestieri, T.Usui, A.Stroppa, A.Bergman, L.Bergqvist, D.Prabhakaran, O.Eriksson, S.Picozzi, T.Kimura and J.Lorenzana, *Phys. Rev.B,* 2014, **90,** 014437

49 J D. Makinson, J.S. Lee, S.H. Magner, R.J. De Angelis, W.N. Weins, and A.S.Hieronymus, *Advances in X-ray Analysis,* 2000, **42**, 407

50 Ji-Wook Yoon, Hyo-Joong Kim, Il-Doo Kim and Jong-Heun Lee, *Nanotechnology*, 2013, **24,** 444005

51 J.Lim, S.P.Yeap, H.X.Che and S.C.Law, *Nanoscale Res. Lett*. 2013, **8**, 381

52 J. Li, Scott K. Cushing, P. Zheng, F. Meng, D. Chu and N. Wu, *Nature Comm.,* 2013, **4,** 2651

53 S.Layek and H.C.Verma, *J.Nanosci.Nanotechnol.,* 2013, **13,** 1848

54 Y.Li, M.Xu, L.Pan, Y.Zhang, Z.Guo and C.Bi*, J.Appl.Phys.,* 2010, **107,** 113908

55 J.M.Wesselinowa*, Physics Letters A,* 2011, **375**, 1417

56 T. N. Shendruk, R. D. Desautels, B. W. Southern, and J. van Lierop, *Nanotechnology,* 2007, **18,** 455704

57 K. O. Moura, R. J. S. Lima, A. A. Coelho, E. A. Souza-Junior, J. G. S. Duque, and C. T. Meneses, *Nanoscale,* 2014, **6,** 352

58 K. R. Deepthi, T. Pandiyarajan and B. Karthikeyan, *J Mater Sci: Mater Electron,* 2013, **24,** 1045

Fe-induced morphological transformation of 1-D CuO nanochains to porous nanofibers with enhanced optical, magnetic and ferroelectric properties

Umesh Kumar Gaur, Anil Kumar and G.D.Varma

The doping of Fe to 1-D CuO nanochains induces their morphological transformation to nanofibers with enhanced multifunctional properties, suggesting their potential for applications in microelectronics and memory devices.